PERSPECTIVE ON THERMAL CREEP AND HYDRIDE ORIENTATION FOR DRY STORAGE AND TRANSPORTATION APPLICATIONS

A.J. MACHIELS
Albert Machiels Consulting
Brentwood, California, USA
Email: ajmachiels@gmail.com

K.P. WALDROP
Electric Power Research Institute, Inc.
Palo Alto, California, USA

P. RUDLING
Advanced Nuclear Technology International
Tollered, Sweden

Abstract

Two potential cladding degradation mechanisms have been the focus of regulatory authorities' reviews when evaluating applications for storage and transportation of spent nuclear fuel under dry, inert atmosphere conditions: thermal creep and hydride re-orientation. A review of the thermal creep mechanisms in the low and high stress regions and their dependence on applied stress, as supported by experimental work, leads to the conclusion that creep failure is highly unlikely for internally pressurized spent fuel rods. Through a process of elimination, the formation of radial hydrides can be assessed to be minor or completely eliminated for several types of BWR and PWR claddings; claddings that would benefit from additional investigations include RX and pRX PWR claddings when hydride dissolution upon heating occurs in a temperature range sufficiently high for complete hydride dissolution, but too low for any significant radiation damage annealing.

1. INTRODUCTION

Two potential cladding degradation mechanisms have been the focus of regulatory authorities' reviews when evaluating applications for storage and subsequently transportation of spent nuclear fuel under dry, inert atmosphere conditions: thermal creep and hydride re-orientation. With regard to the latter, cladding types will be reviewed for their susceptibility to hydride reorientation and R&D topics will be suggested for closing any remaining gaps.

2. THERMAL CREEP

Thermal creep is the tendency of solid materials, in this case Zr-based cladding alloys, to deform permanently under the influence of temperature and stress, the latter being initially below the yield strength of the material. Excessive deformation can result in rupture.

Systematic cladding failure by creep must be avoided during dry storage. Regulatory requirements seek to minimize the likelihood of creep rupture failures by limiting either:

(a) Maximum allowed temperatures (for example, USA); or
(b) Cladding diametral strain to ≤1% (for example, Germany).

In the U.S. Nuclear Regulatory Commission Standard Review Plan published in 1997 [1], cladding temperatures were allowed to reach 570°C during water removal and vacuum drying, as well as under accident conditions and short-term, off-normal conditions. The basis for 570°C was derived from creep testing conducted on irradiated Zircaloy-4 rods [2]. It was recognized, however, that this 570°C limit was obtained by creep testing of low-burnup fuel rod with low internal fuel-rod gas pressure.

Revision 1 of the Standard Review Plan [3] reflected improved understanding in providing guidance to NRC reviewers. Consistent with Interim Staff Guidance 11, Rev. 3 [4], the revised Standard Review Plan limits peak cladding temperatures to 400°C for all normal operations, including drying. Cladding temperatures up to 570°C can still be justified for short-time loading operations for spent, low-burnup nuclear fuel (SNF) with best-

estimate cladding hoop stress equal to or less than 90 MPa. As a result, previously analyzed SNF did not have to be re-analyzed because that SNF had relatively low burnups with cladding stress likely to be less than 90 MPa. NUREG-1536, Rev. 1 [3] also states that for off-normal and accident conditions, the maximum cladding temperature shall not exceed 570°C. The basis for allowing up to 570°C for off-normal and accident conditions is, at least in part, based on the previously cited work by [2], which showed no cladding rupture after relatively long creep test times of 30 days and 73 days at 571°C.

The more detailed creep discussion in the next sections provides mechanistic support for the limited effect of creep.

2.1. Creep testing

Experimentally, the shape of thermal creep curves, i.e., diametral strain as a function of time, depends on the testing protocol. Given the geometry of fuel rod cladding, only creep testing of tube specimens is considered in the paper. The most common approach for creep testing of cladding tube specimens is by maintaining a constant pressure inside the specimen during the duration of the test ("constant load" protocol). A second approach is to maintain the applied stress by adjusting, if necessary, the internal pressure to account for the changes in tubing dimensions ("constant stress" protocol). The testing protocol that is closest in applicability to fuel rods in dry storage is to pressurize the specimen and seal it at both ends before inserting it into a creep testing furnace ("constant gas content" protocol).

Assuming that the initial testing parameters for these three testing protocols are identical (identical temperature and initial internal pressure values), Fig. 1 provides an illustration of the shape of the three curves that would be expected by testing the same material according to the three different protocols referred to above.

Creep curves are typically described as reflecting up to three stages during the deformation process. The first two stages are Stage I, or primary creep, and Stage II, or secondary creep. Primary creep occurs at the beginning of the test, as shown in Fig. 1 where ε_e and ε_p denotes the instantaneous elastic strain and the transient primary creep strain, respectively. During the transient primary creep stage, the creep strain rate decreases as strain increases until Stage II is reached. In Stage II, or secondary creep, the rate at which the specimen deforms (i.e., the slope of the curve) becomes nearly constant; this stage is referred to as steady-state creep; the secondary creep strain is denoted ε_s in Fig. 1. For the purpose of the discussion, the curve capturing the elastic deformation, primary creep transient and initial stage of the secondary creep is shown to be identical for all three testing protocols; this assumes that changes in internal pressure and specimen dimensions (diameter and wall thickness) remain small in the early phases of creep deformation. However, when changes in specimen dimensions become more significant, the shapes of the curves diverge as testing duration increases:

(a) Constant load conditions: As the tubing specimen deforms, changes in tube dimensions (increases in outside and inside diameters and decrease in wall thickness) result in increasing applied stress levels. The applied stress eventually becomes locally greater than the yield stress, and plastic deformation at the structurally weakest location in the cladding tube eventually results in specimen rupture.

(b) Constant stress conditions: The creep rate (i.e., the slope of the creep curve) remains the same as internal pressure is continuously adjusted, if necessary, for accounting for the changes in specimen dimensions in order to maintain a constant hoop stress in the specimen. Stage II is greatly expanded time-wise until the specimen wall becomes so thin that plastic deformation and rupture occur at the structurally weakest location in the cladding tube.

(c) Constant gas content conditions: When the sealed specimen contains fuel, or more likely dummy fuel pellets, the volume available to the gas content inside the specimen may represent a small fraction of the specimen's internal volume. Such a "fuelled" tube specimen experiences a decreasing stress because the internal specimen void volume available to the gas inventory in the rod increases markedly when the initial void volume is small.

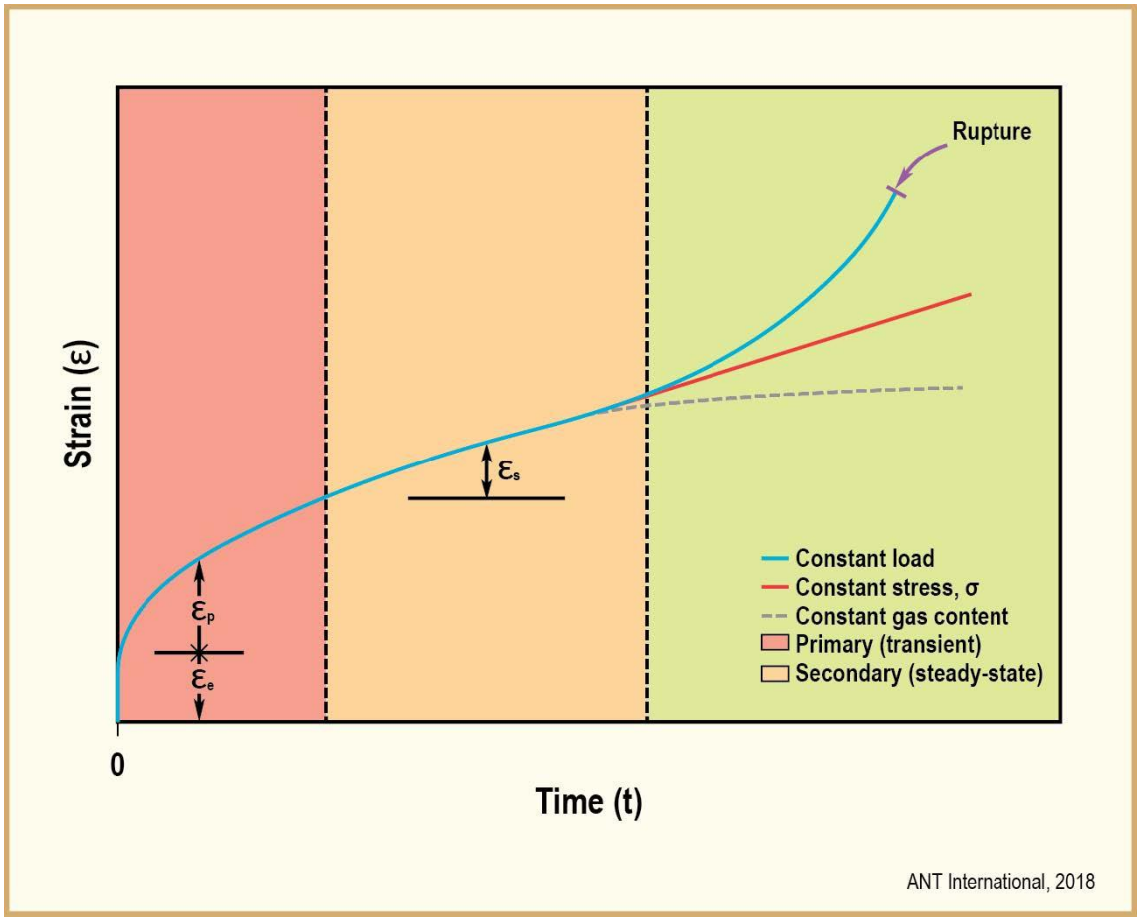

FIG. 1. Typical shapes of creep curves (diametral strain versus time) obtained under constant load, constant stress, and constant gas content conditions.

2.2. Thermal creep deformation mechanisms

Detailed accounts of various creep mechanisms can be found in the literature. Based on the different creep deformation mechanisms and experimental data, Chin et al. [5] developed a secondary creep deformation map for unirradiated, non-hydrided Zircaloy. Secondary creep rates are shown in black lines going across the different deformation kinetics regions in Fig. 2, where ln(σ/E) is plotted against Tm/T:

- Tm is the melting temperature of Zircaloy equal to 2125 K;
- T is the temperature [K];
- σ is the applied stress [MPa];
- E is Zircaloy's Young's modulus equal to (11.09 – 11.61 T/Tm)$_*$104 MPa.

For reference, a constant secondary creep rate of 10^{-10} s^{-1} means that it takes ~3 years to achieve a 1% strain for as-fabricated Zircaloy tubing. Therefore, there is little interest in initial secondary creep rates that are below 10^{-10} s^{-1}, because peak cladding temperature and hoop stresses markedly decrease during the first three years of storage. The resulting drops in temperature and hoop stress over the first three years effectively reduce the initial 10^{-10} s^{-1} secondary creep rate value to levels that are an order of magnitude lower.

By inspection, it can be seen that for normal dry storage conditions (typically, T <673 K and σ <120 MPa), grain boundary sliding and low/high temperature climb dominate. A boundary between two adjacent deformation kinetics regions means the two mechanisms involved contribute equally to the secondary creep strain rate value.

Secondary creep rates can be generically expressed as a function of several parameters. For the purpose of the paper, only the dependence of the secondary strain rate, $\dot{\epsilon}$ on $(\sigma/E)^n$ is retained.

Table 1 lists the mechanisms of greatest interest to dry storage conditions and their dependency on the stress exponent *n* and temperature.

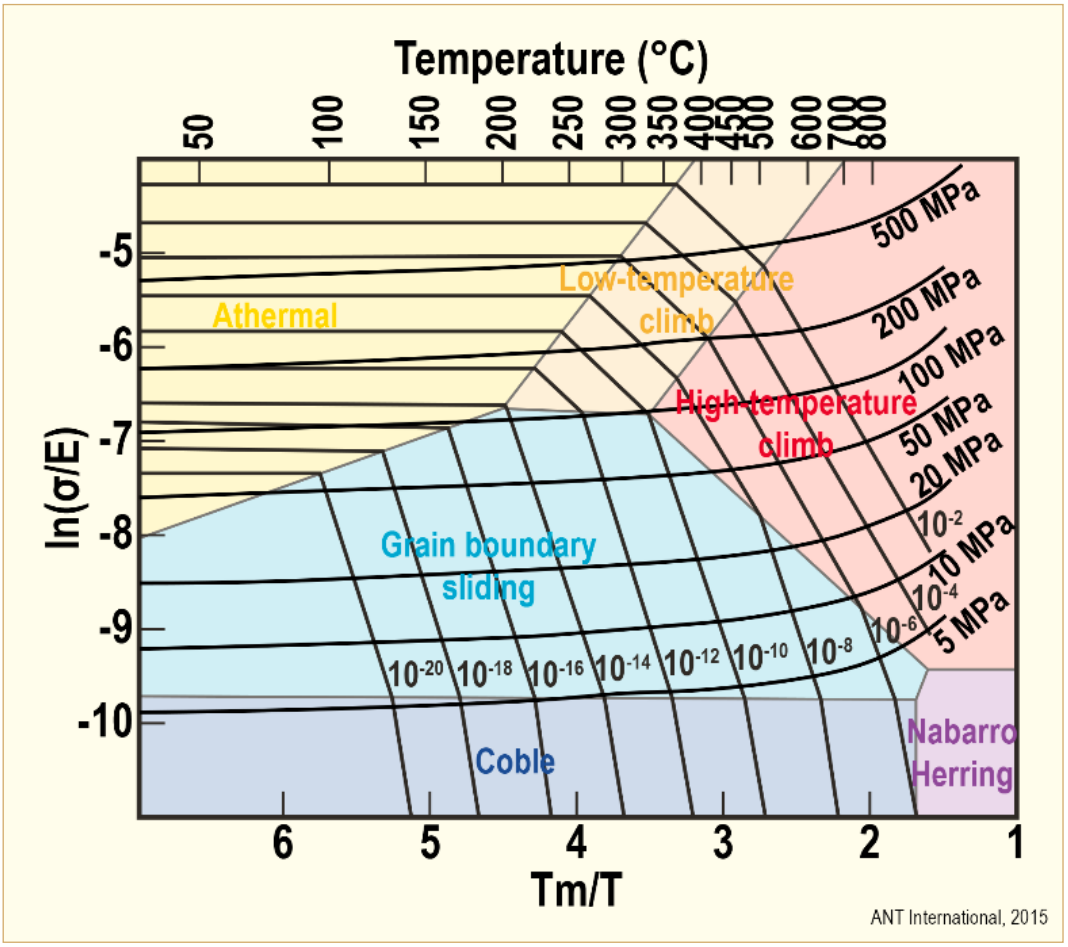

FIG. 2. Deformation map with constant stress and strain rate contours according to [5].

TABLE 1. DOMINANT THERMAL CREEP MECHANISMS

Mechanism	Stress exponent *n*	Temperature dependency
Grain boundary sliding	1-3	Low
Low temperature dislocation climb	3-7	Intermediate
High temperature dislocation climb	7-9	High

2.3. Supporting experimental observations

To illustrate the dependency of thermal creep on the controlling deformation mechanisms identified in the previous section, Fig. 3 presents the secondary creep rate results obtained by Ito et al. [6] for irradiated recrystallized annealed (RXA) Zry-2 and cold-worked stress-relieved annealed (CWSR) Zry-4. The transition from the dominant mechanism (grain boundary sliding) to a different one (dislocation climb) as the applied stress increases is readily apparent. Also, to be noted, are the values of the stress exponent, n, close to ~1 in the low stress region and closer to ~10 in the high stress region.

The time (t) dependency of total creep strain (ε) at stresses below yield stress is often described by a saturated primary strain value (ε_P^S) and a steady state creep rate ($\dot{\varepsilon}_s$):

$$\varepsilon = \varepsilon_P^S + \dot{\varepsilon}_S \, t \tag{1}$$

where t stands for time.

The temperature dependency of the secondary creep deformation is usually expressed by an Arrhenius activation temperature (Qs/R) and the stress dependency by a stress exponent (n) in the relevant creep kinetics domain.

In the JNES formulation, the secondary creep rate is expressed as the sum of the contributions in the low and high stress regions and takes the form:

$$\dot{\varepsilon}_S = \dot{\varepsilon}_{SL} + \dot{\varepsilon}_{SH} \tag{2}$$

With

$$\dot{\varepsilon}_{SL} = A_{SL}\left(\frac{E}{T}\right)\left(\frac{\sigma}{E}\right)^{n_{SL}} exp\left(-\frac{Q_{SL}}{RT}\right) \tag{3}$$

$$\dot{\varepsilon}_{SH} = A_{SH}\left(\frac{E}{T}\right)\left(\frac{\sigma}{E}\right)^{n_{SH}} exp\left(-\frac{Q_{SH}}{RT}\right) \tag{4}$$

where A_{sL} and A_{sH} are constants.

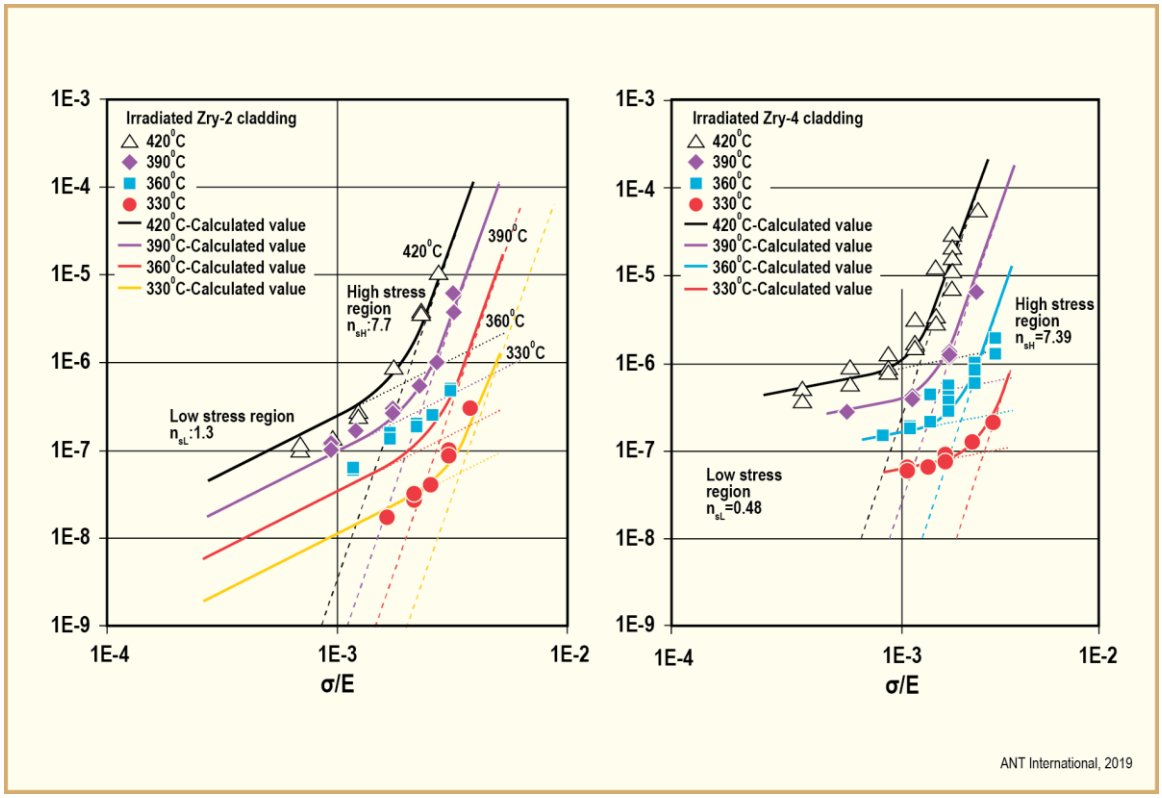

FIG. 3. Secondary creep strain rate [1/h] of RXA Zry-2 (left) and CWRSR Zry-4 from [6].

From regression analyses of the experimental results, the following parameters were obtained [7]:

<u>Irradiated Zry-4 cladding</u>
A_{sL} = 4.04×10^{1} K/MPa/h; n_{sL} = 0.48; Q_{sL} = 109.9×10^{3} J/mol
A_{sH} = 2.50×10^{35} K/MPa/h; n_{sH} = 7.39; Q_{sH} = 297.7×10^{3} J/mol
A_P = 6.58×10^{4} K/MPa; n_P = 1.29; Q_P = 77.2×10^{3} J/mol

Irradiated Zry-2 cladding
A_{sL}=8.12×10^{-2} K/Pa/h; n_{sL}=1.3; Q_{sL}=1.28×10^{5} J/mol
A_{sH}=2.41×10^{26} K/Pa/h; n_{sH}=7.7; Q_{sH}=2.63×10^{5} J/mol
A_p=8.33×10^{-2} K/Pa; n_p=1.3; Q_p=7.71×10^{4} J/mol

Only very few studies, such as those reported by Ito et al. [6] and Kaspar et al. [8], contain tests in the two most relevant stress ranges. Figure 4 plots the ratio of irradiated-to-unirradiated creep rate as a function of hoop stress. In the low stress range, the effect of irradiation is significantly smaller than in the high stress range. The rather small effect of irradiation, which is seen for the data-point of Kaspar et al. [8] at 395°C and a stress of 70 MPa in Fig. 4, can be explained by the rather low fast fluence of this particular sample of 1E20 n/cm² (>1 MeV). All other samples had a much higher fast fluence of 6 to 10E21 n/cm², which is more typical for end-of-life conditions.

Secondary creep rates and creep strains in irradiated cladding are, for all tested temperature conditions and stress regions, smaller than those of unirradiated cladding, but the effect is smaller at lower temperature and lower stress. Irradiation defects such as point defect clusters, interstitial and dislocation loops, etc., create obstacles to dislocation climb. As a result, suppressive effects by irradiation defects are very high in the high stress region. Given that irradiation defects are not considered to be as effective in impacting grain boundary sliding, suppressive effects by neutron irradiation in the low stress region are much less pronounced.

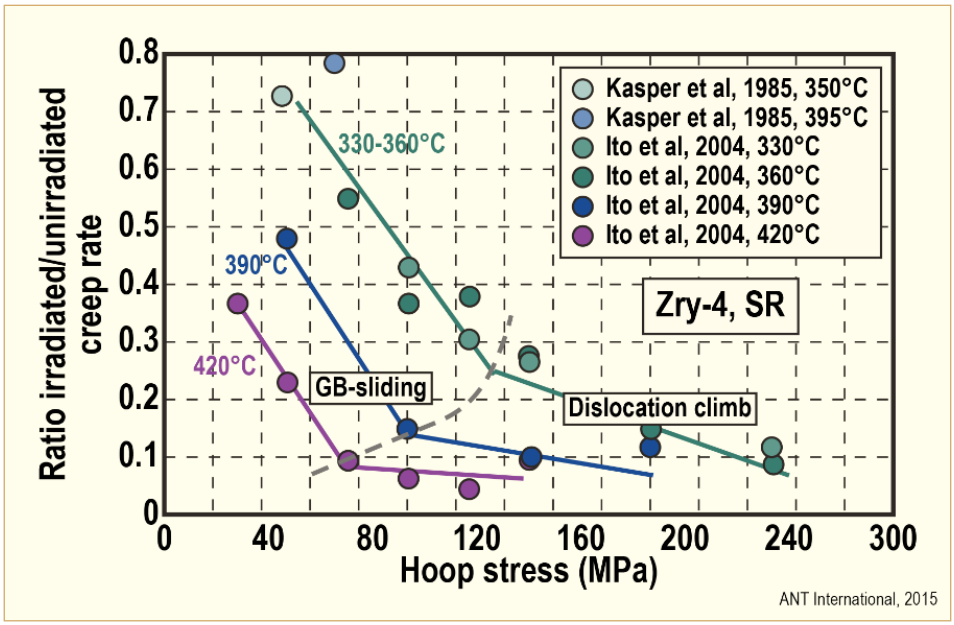

FIG. 4. Stress dependency of the decrease in secondary creep rate after irradiation in comparison to unirradiated CWSR Zry-4 cladding, data from [6] and [8].

2.4. Allowable diametral strain and creep rupture

As previously discussed, regulatory requirements seek to minimize the likelihood of creep rupture failures by either limiting the maximum allowed temperature or by limiting the diametral strain to 1%.

Woodford [9] showed that the strain to creep failure correlates to the stress exponent of secondary creep (Fig. 5). This relationship has been shown to apply to Zr-alloys. From the results obtained by [Ito et al., 2004], the stress exponent, n, varied from 1.3 (RXA Zry-2) and 0.5 (CWSR Zry-4) at low stress to 7.7 (RXA Zry-2) and 7.4 (CWSR Zry-4) at high stress (Fig. 3). Consequently, the failure strain should be ≥100% at low stress and ≥ 10% at high stress for structurally sound rods. Achieving such large strains is not completely unexpected when focusing on the creep curve labeled “Constant Stress” in Fig. 1.

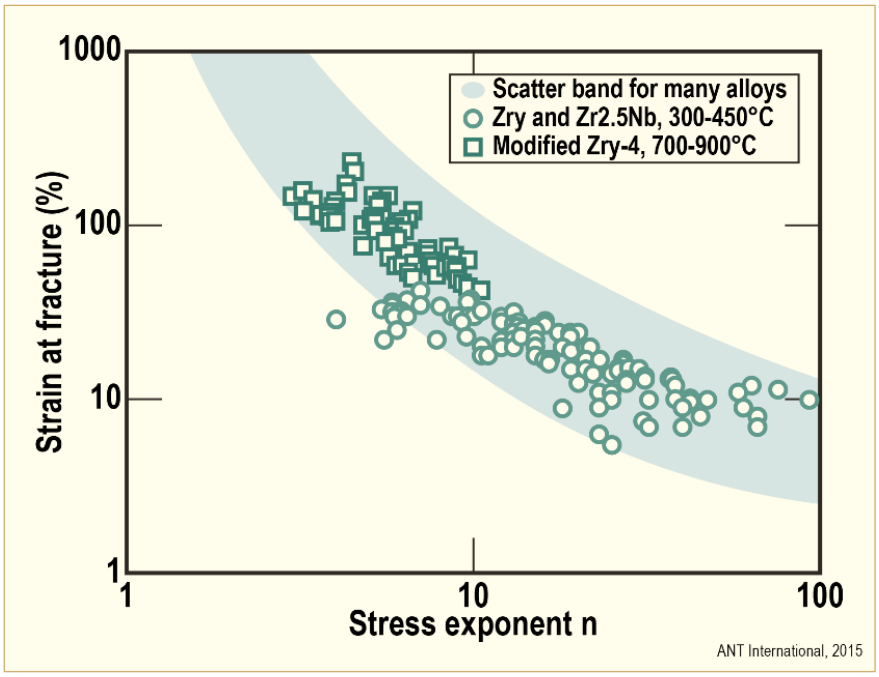

FIG. 5. Creep rupture ductility versus stress exponent of creep n, after [9].

3. HYDRIDE REORIENTATION

Hydride re-orientation refers to a change in hydride lenses stacking orientation that can occur in cladding during the thermal cycle experienced by spent fuel during dry storage. Upon transfer of spent fuel from wet to dry storage, dissolution of zirconium hydrides, possibly up to the hydrogen solubility in the Zr-based alloy, first occurs upon heating. As the fuel slowly cools over time, re-reprecipitation of the hydrides occurs. Depending on alloy characteristics (microstructure, texture, grain shape, …), cladding design (no liner or with inner or outer liner) and condition (hydrogen content, hoop stress level, …), and environmental parameters (temperature, cooling rate, …), alignment of the precipitated hydride lenses may be affected. Prior to dissolution, hydrides are in predominantly circumferential orientation. After reprecipitation, nucleation and growth of radially oriented hydrides are observed when hoop stress levels imposed on cladding specimens are beyond a critical value referred to as the reorientation threshold stress.

3.1. Reorientation threshold stress

Many of the investigations on hydride reorientation measure, or calculate, the threshold hoop stress that results in the first indication of reorientation in spent fuel cladding tubing. Investigations rely on imposing a thermo-mechanical treatment (or hydride reorientation treatment) consisting of heating cladding tube specimens to a high temperature (or peak cladding temperature) followed by cooling while applying, during cooling, an initial hoop stress that can be either kept constant or allowed to decrease with the decreasing temperature. It should be noted that the threshold stress only defines a boundary when some hydride reorientation is first observed; as the magnitude of the applied stress increases above the threshold stress, greater extents of hydride reorientation are observed. Several metrics have been used to characterize the extent of radial-hydride formation. The radial-hydride-continuity factor (RHCF) has been proposed in [10] to better correlate the extent of hydride orientation and morphology with crack initiation and growth during ring compression testing of a cladding specimen that had been subjected to a hydride reorientation treatment [10].

The presence of radial hydrides can result in a degradation of the cladding's mechanical properties, with emphasis on ductility and fracture toughness, when applied stress and hydride orientation are perpendicular to each other. Radial hydrides have no meaningful impact when applied stress and orientation are parallel to each other [11].

Radial hydrides have little impact on cladding fracture properties as long as the fracture strength of the hydrides is larger than the strength of the cladding alloy [12]. According to [12], the fracture strength of the hydrides is about 710 MPa, and, as a first approximation, independent of temperature in the temperature range of interest to dry storage (typically, room temperature to ≤ 400 °C), while the strength of Zircaloy claddings, for example, significantly decreases with increasing temperature from > 800 MPa at 25 °C to ≤ 600 MPa at 400 °C [13]. Therefore, mechanical testing, such as ring compression testing, at different temperatures of cladding alloys containing high levels of radial hydrides can reveal a shift from brittle to ductile fracture, corresponding to the shift from alloy strength greater than hydride fracture strength to alloy strength becoming smaller than hydride fracture strength.

Unlike CWSR claddings, RX claddings have a relatively low strength prior to irradiation; however, after irradiation and pickup of hydrogen resulting from corrosion, radiation hardening and hydrogen embrittlement cause both RX and CWSR claddings to have similar strengths. At room temperature, irradiated CWSR and RX cladding strengths can be significantly higher than the hydride fracture strength. In this case, a ductile to brittle transition (DBT) can be mapped out in claddings characterized by large enough RHCFs; this defines a temperature range between room temperature and the DBT temperature where ductility is low and fracture brittle. However, for RX claddings, if the peak cladding temperature and time at temperature of the hydride reorientation treatment are both high and long enough, annealing of radiation damage can restore the strength of the RX claddings closer to what it was before irradiation, i.e., much lower. Brittle cracking could then be averted, even at room temperature for claddings whose hydrogen content is low enough, due to their strength being now significantly smaller than the fracture strength of the hydrides.

3.2. BWR claddings

The preponderance of BWR cladding designs use an inner liner made of weakly alloyed zirconium. Such designs are not susceptible to hydride reorientation because cooling rates, typically $<3x10^{-3}$ °C/h during dry storage, enable diffusion of hydrogen out of the cladding alloy matrix (typically, Zircaloy-2) and segregation of the hydrogen in the inner liner as a result of the lower solubility of hydrogen in the inner liner compared to that of the alloy matrix [14]. It should also be noted that duplex PWR claddings with outer corrosion-resistant layers would be expected to offer the same protection against hydride reorientation in the meat of the cladding alloy (typically, Zircaloy-4). Barberis et al. concluded from thermodynamics computations that the H chemical potential of Zr alloys increases with Sn [15]. This means that H tends to migrate from higher hydrogen solubility regions (Zircaloy-2 or -4) toward lower hydrogen solubility regions (weakly alloyed Zr in BWR liner or Sn-free corrosion-resistant in PWR outer liner) because of the differences in hydrogen equilibrium concentration.

BWR cladding designs with no inner liner should be considered highly susceptible to hydride orientation when they use RX Zircaloy-2. This is reflected in the JNES recommendations [16]. The latter recommend maximum (peak) cladding temperature ≤ 200 °C and hoop stress ≤ 70 MPa in order to rule out ductility degradation due to hydride reorientation for BWR RX Zircaloy-2 with no inner liner. The limiting temperature of 200 °C limits dissolution (and therefore potential reorientation) of the hydrides to less than 20 wppm. The 70-MPa hoop stress limit was extracted from Aomi et al.'s data [17] showing that a hydride reorientation treatment consisting of heating at 250 °C following by cooling under a constant hoop stress equal to 70 MPa at a cooling rate of 30 °C/h did not result in a change of the Zircaloy-2 ductility.

3.3. PWR claddings

PWR claddings include designs consisting of CWSR alloys and more recent designs consisting of recrystallized (RX) or partially recrystallized (pRX) alloys. These two classes of designs have different microstructure and will be considered separately.

3.1.1 CWSR claddings

Several of the previous investigations on irradiated PWR claddings have focused on CWSR Zircaloy-4 and ZIRLO™. A recent publication [18] helps in connecting results from past investigations. The results from Lee et al. obtained on unirradiated CWSR Zircaloy-4 cladding tube are illustrated in Fig. 6. Shown are the effects of peak cladding temperature and concentration of hydrogen in solid solution, C_{ss}, on reorientation threshold stress and RHCF. The following qualitative behaviours are shown:

— At a given peak cladding temperature, the threshold reorientation stress is at a minimum for Css = TSSD; at 350 °C and 400 °C, the TSSD is equal to ~132 wppm and ~210 wppm, respectively [19]. The threshold increases monotonically as Css decreases when Css is < TSSD; it increases first and then tends to level off when Css increases when Css is > TSSD;
— The threshold stress decreases when the peak cladding temperature increases.

Also plotted is the Radial Hydride Continuity Factor, or RHCF, as determined on etched cross sections of the cladding specimens after hydride reorientation treatment.
The RHCF data show the opposite trends as a function of C_{ss} compared to the reorientation threshold stress.

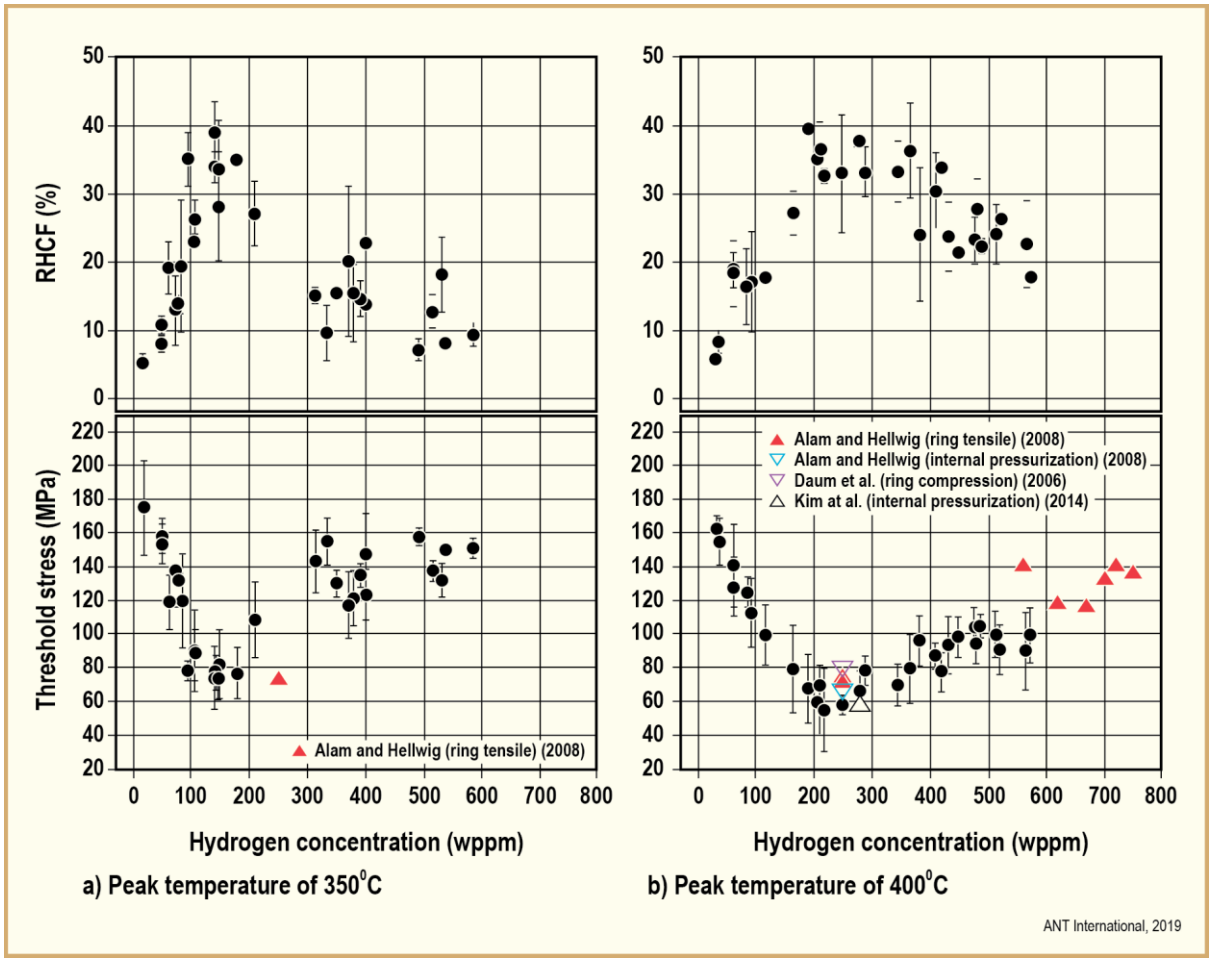

FIG. 6. Hydrogen concentration-dependent threshold stress and RHCF (Adapted from [18]

Such trends appear to be generally consistent with data reported in the open literature. However, the absolute values of threshold stress and RHCF will depend on several factors, such as specimen conditions, as well as on imposed hydride reorientation treatment parameters, such as cooling under constant or decreasing stress and cooling rate.

Past and more recent investigations in assessing and measuring rod internal pressures, and consequently hoop stresses, in discharged spent CWSR claddings result in hoop stresses <100 MPa [20] [21], which would be close to Lee et al.'s threshold stress values at 400 °C, assuming 300-500 wppm in hydrogen content, and below those at 350 °C. For such CWSR claddings, there is less interest in hydrogen content smaller than 200 to 300 wppm, because these claddings tend to have high oxidation layers and high hydrogen content after in-reactor PWR duty. It should be noted that the low rod internal pressures and resulting hoop stress may not be valid for a small fleet of PWRs that routinely discharge fuel with rod-average burnup greater than 62 GWd/MTU.

3.1.2 RX and pRX claddings

More recent PWR cladding formulations contain Nb and are produced with RX and pRX microstructures. These new claddings have shown to have significantly higher corrosion resistance than Sn-containing CWSR claddings considered in the previous section. Therefore, the greater interest is in the low hydrogen content side of the curves in Fig. 6. RX microstructures have a higher susceptibility to radial hydride formation because of the shape of the alloy grains and resulting orientation of grain boundaries, which can promote nucleation of hydrides. Although there is presently no published data similar to Figure 6 for RX and pRX claddings, it can be rationalized that the curves would have similar shapes with lower values for the threshold stresses at C_{ss} = TSSD. Such shapes can be expected based on the competition between radial hydride nucleation and growth of existing radial or circumferential hydrides, and lower threshold stresses would be expected based on grain shape.

However, peak cladding temperatures as high as 350 and 400 °C would result in some or all of the radiation damage being annealed; this would lower the alloy strength below the hydride fracture strength. When this is the case, radially oriented hydrides will not significantly impact the mechanical and fracture properties of the cladding, as shown in [22] for M5, even when the radial hydrides have RHCF that are close to 100% of the cladding wall thickness [22]. Therefore, the more interesting temperature range to investigate is in the 300 to 325 °C range, where (1) the cladding hydrogen content, C_{ss}, can be equal to or lower than the TSSD in that lower temperature range (75 wppm < TSSD < 100 wppm), and (2) taking into account that significant radiation damage annealing is not expected in this temperature range.

4. SUMMARY

The paper examined two degradation mechanisms, thermal creep and hydride re-orientation, which have been the focus of regulatory authorities' reviews when evaluating applications for storage and subsequently transportation of spent nuclear fuel under dry, inert atmosphere conditions.

4.1. Thermal creep

Thermal creep of cladding tubes under low and high stresses are governed by different mechanisms. As a result, the parameters affecting creep, such as stress and temperature depend on the dominant creep mechanism, which itself is a function of stress and temperature. Information on long-term creep under dry storage conditions at the expected stress of SNF cladding should preferably be deduced from long-duration tests in both the high and low stress range.

The secondary creep rate and creep strain of irradiated cladding are, for all tested temperature conditions and stress regions, smaller than those of unirradiated cladding. However, the effect is smaller at lower temperature and lower stress, where grain boundary sliding mechanism dominates.

In some regulatory regimes, a 1% diametral strain criterion is specified as the maximum allowable strain during dry storage. Failure strain depends on the stress exponent. In the relevant stress range (<120 MPa), rupture strains are likely to be at least one order of magnitude greater than the 1% diametral strain criterion.

In addition to the decrease of temperature over time, any increase in void volume due to creep would also result in a decrease of cladding hoop stress. Thermal creep is a self-limiting mechanism in a closed system such as a fuel rod.

The potential for creep rupture during dry storage can be ruled out except possibly for rods with large and localized cladding defects characterized by excessive, localized wall thickness reduction due to grid-to-rod fretting, hydride blisters, large incipient cracks, or possibly others.

4.2. Hydride reorientation

Through a process of elimination, the formation of radial hydrides can be assessed to be minor or completely eliminated for the following claddings:

— BWR cladding designs with inner liners and duplex PWR cladding designs with outer corrosion-resistant layers;
— BWR and PWR CWSRA claddings irradiated in today's reactors discharging fuel with maximum rod-average burnup of ~62 GWd/MTU, because of low rod internal pressures in discharged fuel rods.

Recrystallized or partially recrystallized BWR (with no inner liner) and PWR claddings may be more susceptible to hydride reorientation. However, the impact of radial hydrides on mechanical properties is minimal, if any, when peak cladding temperatures and time at high temperature are both high and long enough during dry storage, resulting in annealing of radiation damage. There presently remains some lack of experimental verification in the open literature for the impact of radial hydrides in RX or partially recrystallized (pRX) alloys when hydride dissolution upon heating and reprecipitation upon cooling occur in a temperature range sufficiently high for complete hydride dissolution, but too low for any significant radiation damage annealing.

ACKNOWLEDGMENTS

The thermal creep work was sponsored by Advanced Nuclear Technology International (ANT International) and the hydride reorientation work by the Electric Power Research Institute (EPRI).

REFERENCES

[1] NATIONAL REGULATORY COMMISSION, Standard Review Plan for Dry Cask Storage Systems, U.S. Nuclear Regulatory Commission, Washington, DC (1997).
[2] EINZIGER R.E., S. D. ATKIN, D.E. STELLRECHT and V. PASUPATHI., High Temperature Post-irradiation Materials Performance of Spent Pressurized Water Reactor Fuel Rods under Dry Storage Conditions, Nuclear Technology **57** (1982).
[3] NATIONAL REGULATORY COMMISSION, Standard Review Plan for Spent Fuel Dry Storage System at a General License Facility, Final Report, Office of Nuclear Material Safety and Safeguards, U.S. Nuclear Regulatory Commission, Rockville, Maryland, Revision 1 (2010).
[4] NATIONAL REGULATORY COMMISSION, Staff Interim Guidance 11, Revision 3, Cladding Considerations for the Transportation and Storage of Spent Fuel, Rockville, Maryland, USA (2013).
[5] CHIN, B.A., KHAN, M.A. TARN, J.C.L., Deformation and fracture map methodology for predicting cladding behaviour during dry storage, PNL Report 5998 (1986).
[6] ITO, K., KAMIMURA, K., TSUKUDA, Y., Evaluation of Irradiation Effects on Spent Fuel Cladding Creep Properties, International Meeting on LWR Fuel Performance, Orlando, Florida, USA American Nuclear Society (2004).
[7] INTERNATIONAL ATOMIC ENERGY AGENCY, Spent Fuel Performance Assessment and Research: Final Report of a Coordinated Research Project (SPAR-II), IAEA-TECDOC-1680, IAEA, Vienna (2012).
[8] KASPAR, G., PEEHS, M., STEINBERG, E., Experimental Investigation of post pile creep of Zircaloy cladding tubes, 8th SMIRT Conference, Brussels, Belgium (1985).
[9] WOODFORD, D.A., Strain Rate Sensitivity as a Measure of Ductility, Transactions of the ASM **62** (1969) 291-293.

[10] BILLONE, M.C., BURTSEVA, T.A., EINZIGER, R.E., Ductile-to-brittle transition temperature for high-burnup cladding alloys exposed to simulated drying-storage conditions, J. Nucl. Mater **433** (2013).

[11] YAGNIK, S., KUO, R.C., RASHID, Y.R., MACHIELS, A.J., YANG, R.L., Effect of Hydrides on the Mechanical Properties of Zircaloy-4, ANS Topical Meeting on LWR Fuel Performance, Orlando, FL (2004).

[12] KUBO, T., KOBAYASHI, Y., UCHIKOSHI, H., Determination of fracture strength of δ-zirconium hydrides embedded in zirconium matrix at high temperatures, Journal of Nuclear Materials **435** (2013).

[13] GEELHOOD, K., BEYER, C., LUSCHER, W., Stress/Strain Correlation for Zircaloy, Battelle Pacific Northwest Laboratory, Springfield, Virginia (2008).

[14] AUZOUX, Q., BOUFFIOUX, P., MACHIELS, A.J., YAGNIK, S., BOURDILIAU, B., MALLET, C., MOZZANI, N., COLAS, K., Hydride reorientation and its impact on ambient temperature mechanical properties of high burn-up irradiated and unirradiated recrystallized Zircaloy-2 nuclear fuel cladding with an inner liner, Journal of Nuclear Materials **494** (2017).

[15] BARBERIS, P., VAUGLIN, C., FREMIOT, P., GUERIN, P., Thermodynamics of Zr alloys: application to heterogeneous materials, ASTM International Symposium on Zirconium in the Nuclear Industry, Hyderabad, ASTM STP 1543 (2015).

[16] KAMIMURA, K., Integrity Criteria of Spent Fuel for Dry Storage in Japan, International Seminar on Spent Fuel Storage (ISSF) Tokyo (2010).

[17] AOMI, M., BABA, T., MYASHITA, T., KAMIMURA, K., YASUDA, T., SHINOHARA, Y., TAKEDA, T., Evaluation of hydride reorientation behavior and mechanical properties for high-burnup fuel-cladding tubes in interim dry storage, Journal of ASTM International **5** 9 (2008).

[18] LEE, J-M., KIM, H. A., KOOK, D. H., KIM, Y. S., A study on the effects of hydrogen content and peak temperature on threshold stress for hydride reorientation in Zircaloy-4 cladding, Journal of Nuclear Materials **509** (2018) 285-294.

[19] KAMMENZIND, B., FRANKLIN, D., PETERS, H., DUFFIN, W., Hydrogen Pickup and Redistribution in Alpha-Annealed Zr-4, Zirconium in the Nuclear Industry: 11th International Symposium; ASTM STP-1295 (1996) 338 – 370.

[20] MACHIELS, A.J., RASHID, Y.R., LYON, W.F., SUNDERLAND, D.J., Characterization of end-of-life rod internal pressure in PWR fuel, Nuclear Engineering and Design **324** (2017) 250–259.

[21] RICHMOND, D.J., GEELHOOD, K.J., FRAPCON Analysis of Cladding Performance during Dry Storage Operations (2017) Water Reactor Fuel Performance Meeting, Jeju Island (2017).

[22] BOUFFIOUX, P., AMBARD, A., MIQUET, C., CAPPELAERE, A., AUZOUX, Q., BONO, M., RABOUILLE, O., ALLEGRE, S., CHABRETOU, V., SCOTT, C.P., Proc. Int. LWR Fuel Performance Meeting. TopFuel 2013, Charlotte, North Carolina, United States, Paper #8557.